JOURNAL OF SOLID STATE CHEMISTRY 71, 196–204 (1987)

New Double Chloride in the LiCl–$CoCl_2$ System

II. Preparation, Crystal Structure, Phase Transformation, and Ionic Conductivity of Li_2CoCl_4 Spinel

R. KANNO,* Y. TAKEDA, A. TAKAHASHI, AND O. YAMAMOTO

Department of Chemistry, Faculty of Engineering, Mie University, Tsu, 514 Japan

AND R. SUYAMA† AND S. KUME

College of General Education, Osaka University, Osaka, 560 Japan

Received July 22, 1986; in revised form December 5, 1986

A new double chloride Li_2CoCl_4 was prepared in the LiCl–$CoCl_2$ system and was characterized by X-ray Rietveld structure analysis, differential thermal analysis, high-temperature X-ray diffraction, and electrical conductivity measurements. This phase has an orthorhombic symmetry *Imma*, with lattice parameters $a = 7.1772(2)$, $b = 7.2478(2)$, and $c = 10.2785(3)$ Å, and its unit cell is related to the parent cubic spinel lattice in the manner that $a_o \sim \frac{1}{2}^{1/2}a_c$, $b_o \sim \frac{1}{2}^{1/2}a_c$, and $c_o \sim a_c$, where the subscripts c and o stand for the cubic and orthorhombic structures, respectively. The orthorhombic distortion, caused by a 1 : 1 ordering of Li^+ and Co^{2+} ions on the octahedral sites, transformed to the cubic spinel structure at 308°C. The transition is the order–disorder type for cation distribution on the octahedral sites. Li_2CoCl_4 showed a high ionic conductivity of 5.0×10^{-2} S cm^{-1} at 400°C. The transition from the orthorhombic to the cubic spinel structure corresponds to that from the low to high ionic conductive phase.

Introduction

In a previous paper (*1*), we described the synthesis of new compounds Li_2CoCl_4 and Li_6CoCl_8 in the LiCl–$CoCl_2$ system. Li_6CoCl_8 has the Mg_6MnO_8-type structure which corresponds to a superstructure of the LiCl type with the ordered arrangement of cations and vacancies over the octahedral sites. We also suggested that Li_2CoCl_4 had a related spinel structure from X-ray diffraction measurements, whose pattern showed a close resemblance to those of cubic chloride spinels, Li_2MCl_4 (M = Mg, Mn, Fe, Cd) (*2*). The lattice distortion, however, was observed in Li_2CoCl_4.

Recent studies on chloride spinels Li_2MCl_4 (M = Mg, V, Mn, Fe, Cd) have shown a high lithium ion conductivity at moderate temperature (*3–7*). The compounds were reported to have the inverse spinel structure (*2*) in which half of the lithium ions are tetrahedrally surrounded by chloride ions, and the other half, together with the M^{2+} ions, are distributed statistically over the octahedral sites. The chloride spinels have a high ionic conductivity of around 0.1 sec cm^{-1} at 400°C. The values of the conductiv-

* To whom correspondence should be addressed.

† Present address: Shinnippon Steel Corp., Central R & D Bureau, R & D Laboratories-1, Materials Research Lab.-1, Kawasaki, Japan.

0022-4596/87 $3.00

ity at elevated temperatures are comparable to or more than those for the high lithium ion conductors reported previously.

The ionic conductivity in the spinels was reported to decrease by lattice distortions. The lithium bromide spinels which have the distorted spinel structure showed a higher activation energy for conduction and a lower ionic conductivity than those of the cubic chloride spinels (*8*). For the chloride spinels, on the other hand, all the spinels reported previously have the cubic inverse spinel structure with the space group *Fd3m* except Li_2CoCl_4.

In this report, we determine the crystal structure of Li_2CoCl_4 by X-ray powder Reitveld analysis. The ionic conductivity and the phase transition are also reported and discussed in comparison with those of the chloride spinels, Li_2MCl_4 (M = Mg, Mn, Fe, Cd).

Experimental

The samples were prepared in the same manner as described previously (*1*). X-ray diffraction patterns of the powdered samples were obtained using monochromated Cu$K\alpha$ radiation and a scintillation detector. A high-power X-ray powder diffractometer (Rigaku RAD 12 kW) was used to determine the lattice distortion. A sample holder with an aluminum window 7 μm thick to prevent attack by moisture during measurement was used.

X-ray powder diffraction data for Reitveld analysis were collected on a polycrystalline sample of Li_2CoCl_4 with Cu$K\alpha$ radiation using a high-power X-ray powder diffractometer equipped with a graphite monochromator. The sample was kept under He atmosphere during measurement. Diffraction data were collected by step scanning over an angular range of $10° < 2\theta < 100°$ in increments of 0.02° at room temperature.

The structural refinement of X-ray data was performed using the Rietveld analysis computer program RIETAN provided by Izumi (*9*). Reflection positions and intensities were calculated for both Cu$K\alpha_1$ (λ = 1.5405 Å) and Cu$K\alpha_2$ (λ = 1.5443 Å) with a factor of 0.5 applied to the latter's calculated integrated intensities. The profile function was a pseudo-Voigt function with the mixing parameter γ included in the least-squares refinement.

The high-temperature phases were examined using a high-temperature X-ray diffractometer. The diffraction patterns were taken in a dry nitrogen atmosphere. Silicon powder was used as an internal standard to determine the lattice parameters. Differential thermal analysis (DTA) was carried out for the samples sealed in silica glass containers under vacuum. α-Al_2O_3 was used as a standard. The heating and cooling rates were 1.5°C/min.

The electrical conductivities were measured in the temperature range between room temperature and 500°C in a dry argon gas flow. A sample of about 0.5 g was pressed into pellets. Blocking electrodes were deposited on both sides on the pellets by evaporating gold. The conductivity was obtained by ac impedance measurements using a HP4800A vector impedance meter over a frequency range of 5 Hz–500 kHz. The resistances were derived by interpretation of complex impedance plane diagram of the data.

Experimental Results and Discussion

Synthesis and X-Ray Characterization

In the previous paper, we reported the new intermediate compound with the content of 33.3 mole% $CoCl_2$ (Li_2CoCl_4) (*1*). The diffraction pattern of Li_2CoCl_4 showed a strong resemblance to the cubic chloride spinels Li_2MCl_4 (M = Mg, Mn, Fe, Cd). Some lines, however, partially split into doublets. The diffraction pattern was found

to be indicative of an orthorhombic cell with $a_o \sim b_o \sim \sqrt{2}a_c$, and $c_o \sim a_c$, where the subscripts o and c represent the orthorhombic and cubic unit cells, respectively. The brief description of the line splittings is as follows: $(440)_c \rightarrow (004)_o$ and $(220)_o$, $(222)_c \rightarrow (202)_o$ and $(022)_o$, and $(440)_c \rightarrow (400)_o$, $(224)_o$ and $(040)_c$. The cell constants are $a = 7.177$, $b = 7.247$, and $c = 10.278$ Å. The orthorhombic cell could be related to the cubic spinel as follows:

$$\begin{pmatrix} a_o \\ b_o \\ c_o \end{pmatrix} = \begin{pmatrix} \frac{1}{2} & \frac{1}{2} & 0 \\ -\frac{1}{2} & \frac{1}{2} & 0 \\ 0 & 0 & 1 \end{pmatrix} \begin{pmatrix} a_c \\ b_c \\ c_c \end{pmatrix}$$

The observed and calculated d values are listed in Table I. Diffraction extinctions were observed as follows: hkl presents only with $h + k + l = 2n$, $hk0$ only with $h = 2n$, and $k = 2n$, $0kl$ only with $k + l = 2n$, $h0l$ only with $h = 2n$ and $l = 2n$, $h00$ only with $h = 2n$, $0k0$ only with $k = 2n$, and $00l$ only with $l = 2n$. They are characteristic of the space groups *Imma* and *Ima*2.

TABLE I

X-RAY DIFFRACTION DATA OF Li_2CoCl_4

$h\,k\,l_{cubic}$	$h\,k\,l_{ortho}$	d_{cal}	d_{obs}	I_{obs}
1 1 1	0 1 1	5.923	5.928	41.2
	1 0 1	5.884	—	—
2 0 0	0 0 2	5.139	5.141	10.7
2 2 0	0 2 0	3.623	3.622	6.0
	1 1 2	3.619	—	—
	2 0 0	3.588	3.589	4.7
3 1 1	0 1 3	3.097	3.096	8.0
	1 0 3	3.091	—	—
	1 2 1	3.085	—	—
	2 1 1	3.069	3.067	17.1
2 2 2	0 2 2	2.961	2.960	20.1
	2 0 2	2.942	2.942	14.2
4 0 0	0 0 4	2.569	2.569	71.9
	2 2 0	2.549	2.550	100.0
3 3 1	1 2 3	2.352	—	—
	0 3 1	2.351	2.350	3.3
	2 1 3	2.344	2.344	
	3 0 1	2.330	—	—
4 2 0	1 1 4	2.294	—	—
	2 2 2	2.284	2.284	3.6
4 2 2	0 2 4	2.096	2.095	1.1
	1 3 2	2.091	—	—
	2 0 4	2.089	2.089	1.6
	3 1 2	2.077	—	—

TABLE I–*Continued*

$h\,k\,l_{cubic}$	$h\,k\,l_{ortho}$	d_{cal}	d_{obs}	I_{obs}
	0 1 5	1.977	1.977	1.0
	1 0 5	1.976	—	—
3 3 3	0 3 3	1.974	1.966	1.8
5 1 1	2 3 1	1.966		
	3 0 3	1.961	—	—
	3 2 1	1.959	—	—
	0 4 0	1.811	1.810	56.0
4 4 0	2 2 4	1.809		
	4 0 0	1.794	1.794	12.2
	1 2 5	1.735	—	—
	2 1 5	1.732	1.730	4.0
5 3 1	1 4 1	1.731		
	2 3 3	1.729		
	3 2 3	1.725	—	—
	4 1 1	1.717	1.717	2.1
	0 0 6	1.713		
6 0 0	1 3 4	1.709	—	—
4 4 2	0 4 2	1.708	1.708	0.7
	3 1 4	1.702	—	—
	4 0 2	1.694	1.691	0.4
	1 1 6	1.623	—	—
6 2 0	2 4 0	1.617	1.617	0.4
	3 3 2	1.613	—	—
	4 2 0	1.607	1.609	0.4
	0 3 5	1.565	1.566	1.1
5 3 3	1 4 3	1.563	—	—
	3 0 5	1.559	—	—
	4 1 3	1.552	1.553	1.1
	0 2 6	1.548	1.548	2.7
6 2 2	2 0 6	1.545	—	—
	2 4 2	1.542	1.542	3.0
	4 2 2	1.534	1.535	3.1
4 4 4	0 4 4	1.480	1.481	10.0
	4 0 4	1.471	1.471	8.3

Hass classified the distortions in the oxide spinel structure from the standpoint of cation ordering in the octahedral (B) and/or tetrahedral (A) sites (*10*). Eight kinds of ordering have been proposed: 1 : 1 order on A site, 1 : 3 order on B site, 1 : 1 order on B site (α and β), 1 : 3 order on B site and 1 : 1 order on A site, 1 : 5 order on B site, 1 : 2

order on *A* site, and hausmanite-type distortion. The orthorhombic distortion was reported for the 1 : 1 order on *B* site (β) with the space group of *Imma*. For Li_2CoCl_4, the 1 : 1 order on the octahedral *B* sites seems to be possible. To confirm this assumption, x-ray diffraction intensity was briefly calculated under the following conditions:

$4e$ $Li(1)_{tetra}$ 0, $\frac{1}{4}$, z; 0, $\frac{3}{4}$, $-z$
$4b$ $Li(2)_{octa}$ 0, 0, $\frac{1}{2}$; 0, $\frac{1}{2}$, $\frac{1}{2}$
$4d$ Co_{octa} $\frac{1}{4}$, $\frac{1}{4}$, $\frac{3}{4}$; $\frac{3}{4}$, $\frac{1}{4}$, $\frac{3}{4}$
$8h$ Cl(1) 0, y, z; 0, $-y + \frac{1}{2}$, z;
0, $y + \frac{1}{2}$, $-z$; 0, $-y$, $-z$
$8i$ Cl(2) x, $\frac{1}{4}$, z; $-x$, $\frac{1}{4}$, $-z$;
$-x$, $\frac{3}{4}$, $-z$; x, $\frac{3}{4}$, $-z$

The positional parameters of z in the $4e$, y and z in the $8h$, and x and z in the $8i$ positions were fixed at $\frac{1}{8}$, 0, $\frac{1}{4}$, $\frac{1}{4}$, and 0, respectively. The calculated pattern was in good agreement with the observed one. Li_2CoCl_4 is then suggested to have the spinel structure or a related spinel structure with the 1 : 1 ordering of Li^+ and Co^{2+} ions on the octahedral sites.

Structure Refinement of Li_2CoCl_4

Refinement of the structure proceeded in a straightforward manner with the space group *Imma*, where centrosymmetry was assumed. The initial coordinates for the structural model were taken as pointed out in the previous section. The refinement was done in stages, with the atomic coordinates and thermal parameters fixed in the initial calculations and subsequently allowed to vary only after the scale, background, half-width, and unit call parameters were close to convergence on their optimum values. Initial refinement using the above positional parameters did not proceed to low *R*-value. We repeated the refinement cycles with an extra condition, taking into account a partial disorder of the Li^+ and Co^{2+} ions on the $4b$ and $4d$ octahedral sites. Refinement proceeded to the agreement factors R_{wp} = 17.89, R_p = 14.09, and R_B = 14.37. (The agreement factors are based on weighted profile fits, profile fits, and Bragg intensities, respectively.) An extraordinarily large Debye–Waller coefficient (23(8) Å^2), however, was observed for the Li^+ ions on the tetrahedral $4e$ sites. Further, the interatomic distance of Li (on $4e$ site)–Cl(1) was calculated to be 1.92 Å, which is much shorter than the sum of the ionic radii for Li^+ and Cl^- ions (2.4 Å). Thus, the tetrahedral $4e$ site is not the suitable position for the Li^+ ions.

For further refinement, we assumed that the Li(1) ions are partially occupied in other positions. Three kinds of positions were then considered around the $4e$ tetrahedral sites: four $16j$ positions which distribute around the $4e$ sites along both ⟨100⟩ and ⟨010⟩ directions, two $8h$ positions which distribute along ⟨100⟩ direction, and two $8i$ positions which distribute along ⟨010⟩ direction. Refinement based on the $8h$ positions did not result in better agreement factors, and that based on the $16j$ positions led to the negative Debye–Waller coefficient on the $16j$ sites. A satisfying refinement was obtained using the $8i$ positions. This refinement proceeded to better agreement factors, R_{wp} = 16.67, R_w = 13.10, and R_B = 12.61, then obtained on other positions. Table II shows the final structural parameters for Li_2CoCl_4. The interatomic distances and bond angles are listed in Table III.

The structure of the low-temperature form of Li_2CoCl_4 is basically derived from the inverse spinel structure. The spinel structure consists of a cubic close-packed anion array with cations occupying, in an ordered manner, one-eighth of the tetrahedral (*A*) sites and one-half of the octahedral (*B*) sites. The cubic chloride spinels Li_2MCl_4 (*M* = Mg, V, Mn, Fe, Cd) have been reported to have the inverse spinel structure in which half of the lithium ions are in *A* sites, and the other half, together with the

TABLE II

RIETVELD REFINEMENT RESULTS FOR Li_2CoCl_4

Scale factor	0.01159(6)
FWHM parameter U	0.28(2)
V	−0.14(1)
W	0.047(3)
Asymmetry parameter	0.29(2)
Gaussian fraction	0.19(1)
FWHM (Gauss)/FWHM (Lorentz)	1.51(7)
Lattice constant a (Å)	7.1772(2)
b (Å)	7.2478(2)
c (Å)	10.2785(3)

			Fractional coordinates			
Atom	Site	Occupancy	x	y	z	B (Å)
Li(1)	8*i*	0.5	0.159(8)	0.25	0.213(9)	−0.6(21)
Li(2)	4*b*	0.826(17)	0	0	0.5	4.5(13)
Co(1)	4*b*	0.174	0	0	0.5	4.5(13)
Li(3)	4*d*	0.174	0.25	0.25	0.75	0.03(15)
Co(2)	4*d*	0.826(17)	0.25	0.25	0.75	0.03(15)
Cl(1)	8*h*	1	0	−0.011(1)	0.2442(1)	1.75(17)
Cl(2)	8*i*	1	0.246(2)	0.25	−0.0086(7)	1.78(15)

M^{2+} ions, are distributed statistically over the octahedral B sites (*2, 11*).

The structure of Li_2CoCl_4, shown in Fig. 1, is an ordered type with the Co^{2+} and half of the Li^+ ions occupying the octahedral B sites. More than 80% of lithium ions on the B sites arrange on the 4*b* sites along the *b* axis and the cobalt ions arrange on the 4*d* sites along the *a* axis. The $CoCl_6$ octahedral are connected to each other along the *a* axis by sharing Cl(1)–Cl(1) edges, while those in Li_6CoCl_8 are isolated in the Mg_6MnO_8-type structure (*1*). The Co–Cl(1) distance of 2.489 Å is slightly longer than the Co–Cl(2) distance of 2.480 Å. These distances correspond well to the Co–Cl distance of 2.50 Å in Li_6CoCl_8.

For the other half of the lithium ions, they distribute statistically on the 8*i* sites, which are placed between the 4*e* tetrahedral (*A* sites for the spinel structure) and the 4*c* interstitial octahedral sites. The arrangement of the 4*e*, 4*c*, and 8*i* sites is shown in Fig. 2. The 8*i* sites arrange along the *a* axis.

Solid Solution of $Li_{2-2x}Co_{1+x}Cl_4$

An increase in the conductivity of the chloride spinels was reported on modifying the structure by introducing cation vacancies. The solid solutions $Li_{2-2x}M_{1+x}Cl_4$, where the substitution of Li^+ by M^{2+} creates cation vacancies, have higher ionic mobility than the stoichiometric spinels (*3, 5–7*).

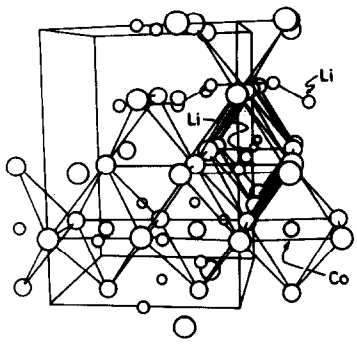

FIG. 1. The structure of Li_2CoCl_4.

TABLE III

BOND LENGTHS AND ANGLES FOR Li_2CoCl_4

	Distance or angle (Å or degree)
Lithium–chlorine tetrahedron	
Li(1) –Cl(1) (×2)	2.24(3)
Li(1) –Cl(1) (×2)	3.12(5)
Li(1) –Cl(2)	2.36(9)
Li(1) –Cl(2)	3.11(9)
Li(1) –Li(1)	2.29(8)
Li(1) –Li(1)	1.50(10)
Li(1) –Li(1) –Li(1)	149(6)
Lithium–chlorine octahedron	
Li(2) –Cl(1) (×2)	2.63(1)
Li(2) –Cl(2) (×4)	2.56(1)
Cl(1) –Li(2) –Cl(2) (×4)	86.6(2)
Cl(1) –Li(2) –Cl(2) (×4)	93.3(2)
Cl(2) –Li(2) –Cl(2) (×2)	89.8(3)
Cl(2) –Li(2) –Cl(2) (×2)	90.1(3)
Cl(1) –Li(2) –Cl(1) (×2)	180
Cl(2) –Li(2) –Cl(2)	180
Cobalt–chlorine octahedron	
Co(1)–Cl(1) (×4)	2.489(4)
Co(1)–Cl(2) (×2)	2.480(7)
Cl(1) –Co(1)–Cl(1) (×2)	92.2(1)
Cl(1) –Co(1)–Cl(1) (×2)	87.7(1)
Cl(1) –Co(1)–Cl(2) (×4)	91.7(5)
Cl(1) –Co(1)–Cl(2) (×4)	88.2(5)
Cl(1) –Co(1)–Cl(1) (×2)	180
Cl(1) –Co(1)–Cl(2)	180

The solid solution $Li_{2-2x}Co_{1+x}Cl_4$ was examined because the substitution of Li^+ by Co^{2+} could produce the cation vacancy. The X-ray diffraction patterns of the samples with $x = 0.1$, 0.2, and 0.33 showed the existence of extra lines due to $CoCl_2$. Further, the samples with $x = 0.05$ and 0.10 had the same lattice parameters as the stoichiometric composition. This shows that the solid solution in the cobalt spinel exists only within a very limited range.

Electrical Conductivity and Phase Transition

Temperature dependence of the conductivity, σ, of Li_2CoCl_4 is shown in Fig. 3. The conductivity of 5.0×10^{-2} S cm^{-1} at

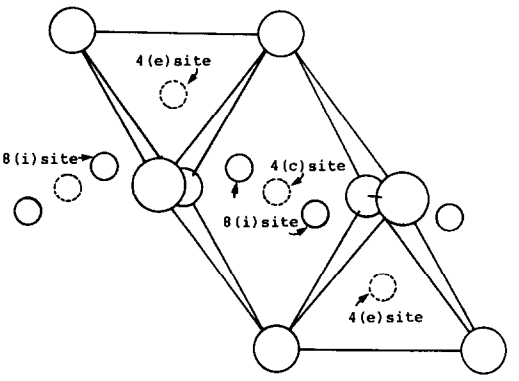

FIG. 2. The arrangement of the 4*e*, 4*c*, and 8*i* sites in Li_2CoCl_4.

400°C is almost comparable to that of Li_6CoCl_8. The Arrhenius plots show a change in slope around 300°C. The activation energies were calculated to be 88 kJ $mole^{-1}$ below the knee and 44 kJ $mole^{-1}$ above the knee in the conductivity curve. The values of activation energies and of conductivities will be discussed in comparison with other

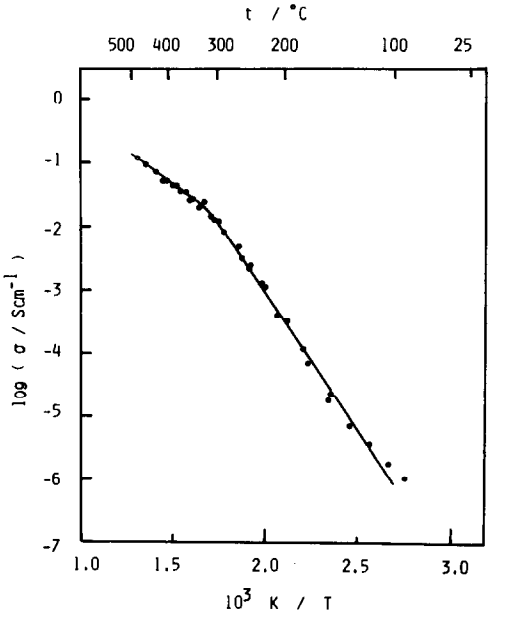

FIG. 3. Temperature dependence of the conductivity of Li_2CoCl_4.

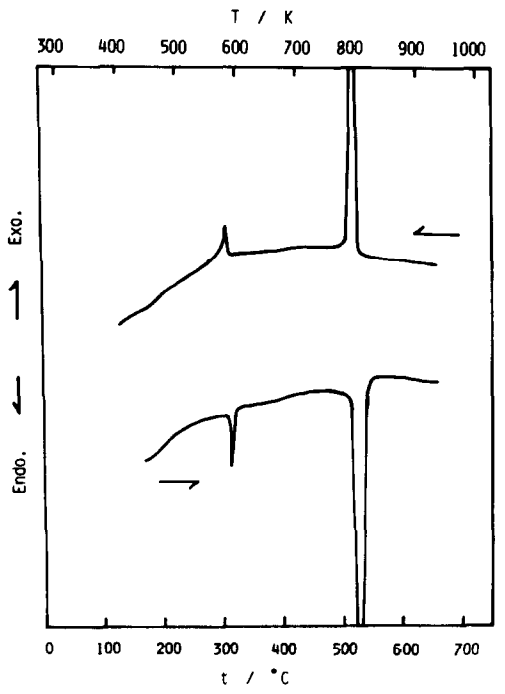

FIG. 4. DTA curves of Li_2CoCl_4.

chloride spinels in a later section of this paper.

The DTA curves of Li_2CoCl_4, shown in Fig. 4, indicated an endothermic peak at 308°C on heating. Figure 5 shows the temperature dependence of the lattice parameters of Li_2CoCl_4 obtained by high-temperature X-ray analysis. The peak splitting due to the orthorhombic distortion disappeared around 300°C, which is in agreement with the transition temperature of 308°C in the DTA curves. The orthorhombic lattice caused by the 1 : 1 cation ordering on *B* sites transformed to the cubic lattice, leading to a random distribution of the Li^+ and Co^{2+} ions on *B* sites. The transition at 308°C can therefore be considered as the order–disorder type about the cation distribution on the octahedral sites. The change in slope in the conductivity curve also corresponds to the transition from the orthorhombic to the cubic structure.

In the previous papers, we reported ionic conductivities of the chloride spinels $Li_{2-2x}M_{1+x}Cl_4$ (M = Mg, Mn, Fe, Cd) (*3, 6, 7*) and of the bromide spinels $Li_{2-2x}M_{1+x}Br_4$ (M = Mg, Mn) (*8*). Figure 6 shows the conductivities and the activation energies of the stoichiometric chloride spinels Li_2MCl_4 (*3, 6, 7*) as a function of ionic radii of divalent metal ions. The ionic radii of the divalent cations are for octahedral environments and those of high spin state are taken for cobalt, manganese, and iron ions. At lower temperatures, these figures show no significant difference in the conductivities or in the activation energies among the spinels except for the cobalt spinel. The low-temperature phase of the cobalt spinel, which was the orthorhombic lattice, shows a considerably lower conductivity and a higher activation energy than the other chloride spinels. At higher temperatures, where all spinels have the cubic structure, no signifi-

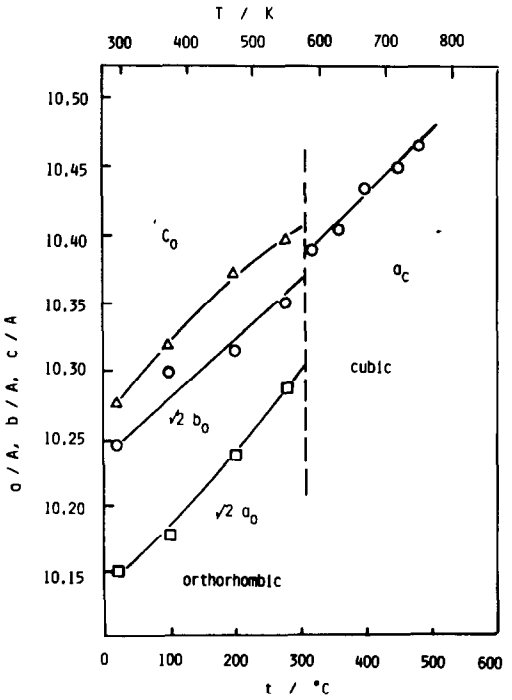

FIG. 5. Temperature dependence of the lattice parameters of Li_2CoCl_4.

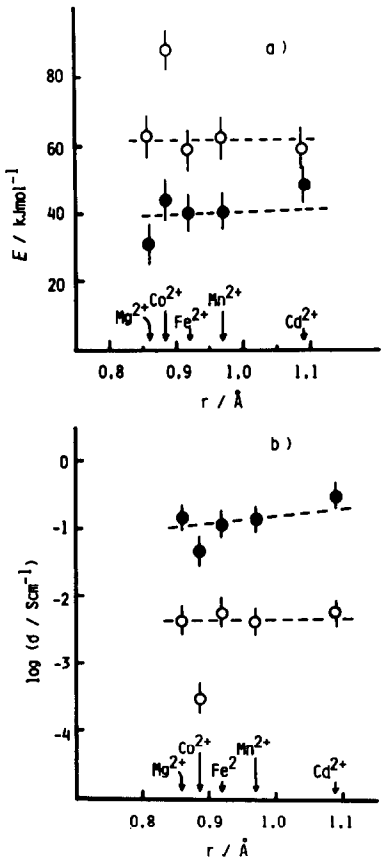

FIG. 6. Activation energies of the chloride spinels Li_2MCl_4 as a function of the ionic radii of divalent metal ions. ○, Activation energies at low temperature; ●, activation energies at high temperature. (b) Conductivities of the chloride spinels Li_2MCl_4 as a function of the ionic radii of divalent ions. ●, Conductivity at 400°C; ○, conductivity at 200°.

cant difference can be observed. This shows that the orthorhombic distortion affects the ionic conduction for the lithium ion.

For the cubic spinel structure, the lithium ions on *A* sites are reported to participate in the ionic conduction. The conduction path is three dimensional along 8*a* tetrahedral–16*c* interstitial octahedral–8*a* tetrahedral sites in Li_2MgCl_4 (*11*). Our refinement results on Li_2CoCl_4, on the other hand, suggest that the ionic conduction in Li_2CoCl_4 is likely due to the motion of lithium ions in the 8*i* sites and that the diffusion pathway is only directed along the *a* axis of the orthorhombic lattice. Furthermore, the 8*i* positions were situated in the octahedron which was the interstitial sites for the cubic spinel structure, as shown in Fig. 2. The differences both in the conclusion path and in the position of the lithium ions may be the reason for that Li_2CoCl_4 has lower ionic conductivities than other cubic spinels.

We measured the ionic conductivities of some fluoride and oxide spinels with lithium in order to make a comparison with those of chloride spinels. The oxides examined in this study were $LiAlTiO_4$ (*12*) and $Li_{4/3}Ti_{5/3}O_4$ (*13*), where the lithium ions occupy the tetrahedral 8*a* sites. For fluoride, only Li_2NiF_4 was reported to have the inverse spinel structure (*14*). In Table IV are summarized the conductivity data. Both of

TABLE IV

CONDUCTIVITY AND CRYSTAL DATA FOR FLUORIDE AND OXIDE SPINELS

Compound	Cation coordination	Lattice parameter,[a] (Å)	Conductivity, σ (S cm^{-1}) 200°C	Conductivity, σ (S cm^{-1}) 400°C	Activation energy, *E* (kJ $mole^{-1}$)
Li_2NiF_4	$(Li)^{IV}[LiNi]^{VI}$	8.3	1.1×10^{-8}	6.2×10^{-6} (at 360°C)	109
$LiAlTiO_4$	$(Li)^{IV}[AlTi]^{VI}$	8.30	5.6×10^{-8}	1.1×10^{-5}	70
$Li_{4/3}Ti_{5/3}O_4$	$(Li)^{IV}[Li_{1/3}Ti_{5/3}]^{VI}$	8.36	—	5.6×10^{-4}	—

these oxides and fluoride showed lower conductivities than the chloride spinels. The lattice parameters of oxides and fluoride spinels are about 8.3 Å, the value of which is comparatively smaller than those of other halide spinels ($a \sim 10$–11 Å). The smaller ionic radii of fluoride (1.19 Å) and oxide (1.26 Å) ions in comparison with those of chloride (1.67 Å) ions are the reason for the small unit cell of fluoride and oxide spinels. The lower conductivities of the oxide and fluoride spinels can be explained by the small bottleneck size of the conduction path, which makes lithium ions less mobile from the tetrahedral to the octahedral interstitial sites.

From the results of conductivity measurements on the halide spinels, the Arrhenius conductivity plots showed a change in slope between 200 and 300°C in all Li_2MX_4 systems (*3–8*). The change in slope is represented by the transition from the low to high conducting state as described in a previous paper (*15*). A neutron diffraction study on Li_2MgCl_4 at higher temperatures showed a gradual displacement of lithium ions from the tetrahedral 8*a* to the interstitial 16*c* sites (*11*). These two sites are almost equally populated above the knee in the conductivity curve. This evolution occurs without any other important change in the structure, particularly on the space group *Fd*3*m* and for the cation distribution on the 16*d* octahedral sites. For cobalt chloride spinels, on the other hand, the crystalline transition from the orthorhombic to the cubic structure corresponds to the change in slope in the conductivity curve. However, the activation energy above the knee in Li_2CoCl_4 is also comparable to that of other chloride spinels (see Fig. 6). This indicates that a disordering state of mobile ions should be expected along the conduction path in the high-temperature cubic cobalt spinel.

Acknowledgments

Reflection intensity measurements were performed at the Materials Analyzing Center at the Institute of Scientific and Industrial Research, Osaka University. We Thank Mr. Tanaka of the center for his assistance with the measurements. All computations for the structure refinement were carried out at the Crystallographic Research Center, Institute of Protein Research, Osaka University. We thank Professors K. Kamiya and T. Yoko at Mie University for the use of the high-temperature K-ray diffractometer and Professor M. Takano at Kyoto University for useful discussions.

References

1. R. Kanno, Y. Takeda, A. Takashi, O. Yamamoto, R. Suyama, and M. Koizumi, *J. Solid State Chem.* **71,** 189 (1987).
2. C. J. J. van Loon and J. de Jong, *Acta Crystallogr. Sect. B* **31,** 2549 (1975).
3. R. Kanno, Y. Takeda, and O. Yamamoto, *Mater. Res. Bull.* **16,** 999 (1981).
4. H. D. Lutz, W. Schmidt, and H. Haeuseler, *J. Phys. Chem. Solids* **42,** 287 (1981).
5. C. Cros, L. Hanebali, L. Latie, G. Villeneuve, and W. Gang, *Solid State Ionics* **9/10,** 139 (1983).
6. R. Kanno, Y. Takeda, and O. Yamamoto, *Solid State Ionics* **9/10,** 153 (1983).
7. R. Kanno, Y. Takeda, K. Takada, and O. Yamamoto, *J. Electrochem. Soc.* **131,** 469 (1984).
8. R. Kanno, Y. Takeda, O. Yamamoto, C. Cros, W. Gang, and P. Hagenmuller, *J. Electrochem. Soc.* **133,** 1052 (1986).
9. F. Izumi, *J. Miner. Soc. Japan* **17,** 37 (1985).
10. C. Haas, *J. Phys. Chem. Solids* **26,** 1225 (1965).
11. J. L. Soubeyroux, C. Cros, W. Gang, R. Kanno, and M. Pouchard, *Solid State Ionics* **15,** 293 (1985).
12. V. G. Keramidas, B. A. Deangelis, and W. B. White, *J. Solid State Chem.* **15,** 233 (1975).
13. M. R. Harrison, P. P. Edwards, and J. B. Goodenough, *J. Solid State Chem.* **54,** 136 (1984).
14. W. von Rudorff, J. Kandler, and D. Babel, *Z. Anorg. Allg. Chem.* **317,** 261 (1962).
15. R. Kanno, Y. Takeda, O. Yamamoto, C. Cros, W. Gang, and P. Hagenmuller, *Solid State Ionics* **20,** 99 (1986).